Korean J. Chem. Eng., 32(10), 2014-2023 (2015)
DOI: 10.1007/s11814-015-0021-2

pISSN: 0256-1115
eISSN: 1975-7220

Preparation of reusable conductive activated charcoal plate as a new electrode for industrial wastewater treatment

Baharak Ayoubi-Feiz and Soheil Aber†

Research Laboratory of Environment Protection Technology, Department of Applied Chemistry, Faculty of Chemistry, University of Tabriz, Tabriz, Iran
(*Received 22 May 2014 • accepted 26 January 2015*)

Abstract−A conductive activated charcoal plate (ACP) was prepared from a low-cost, abundant, and non-conductive charcoal. The prepared ACP was characterized using N_2 adsorption/desorption isotherms, scanning electron microscopy (SEM), Fourier transform infrared spectroscopy (FT-IR) and X-ray diffraction (XRD). Brunauer-Emmett-Teller (BET) surface area of the charcoal and the ACP was 0.58 m^2 g^{-1} and 461.67 m^2 g^{-1}, respectively. The ACP was employed in textile wastewater treatment using electrosorption process. Response surface methodology (RSM) was applied to design the experiments. The decolorization efficiency of 76% at optimum conditions of voltage=450 mV, pH=4, and contact time=120 min indicated that the ACP has promising potential to decolorize textile wastewater. Moreover, the results of the kinetic analyses demonstrated that wastewater treatment followed pseudo-first order kinetic model. The ACP electrode could be regenerated and reused effectively at five successive cycles of electrosorption/electrodesorption.

Keywords: Conductive Activated Charcoal Plate, Electrosorption, Physical Activation, Regeneration, Textile Wastewater

INTRODUCTION

The treatment of wastewater has become a major global challenge. The textile industry, as one of the important water consumers, produces highly colored and complex wastewater [1]. Biological treatment is commonly used for environmental pollutants removal, but it is ineffective in treatment of textile wastewater due to the presence of high concentration of dyes [2]. Among different wastewater treatment methods, adsorption is recognized because of its simple design, easy operation and high pollution removal capacity even from dilute solutions without generation of by-products [3-5]. But, adsorption has some obstacles like long required time and regeneration of used adsorbents [6].

Electrosorption is a potential-induced adsorption method that has none of the mentioned disadvantages of the adsorption [7]. Mechanism of the electrosorption is based on the formation of electrical double-layer within the electrode/electrolyte interface [8]. By applying an electric field between two opposite electrodes, charge separation occurs and charged ions in contaminated solution are forced to move toward the surface of electrode with counter charge [9]. It results in the enhancement of the adsorption rate and capacity. Since the electrosorption runs at low voltages, it can be considered as environmentally friendly [10]. On the other hand, regeneration of used adsorbent by applying a reverse potential (electrodesorption) method is faster and more economical than conventional methods such as thermal regeneration [11]. Accordingly, the electrosorption has been recently proposed as an effective, fast, and simple method to decrease water treatment cost and prevent environmental pollution [12,13].

Activated carbon fiber [14], carbon nano tube [15], graphene [16], and carbon aerogel [17] with large specific surface areas have been used as electrosorption electrodes. However, the manufacturing process of these materials is complicated and their production is very expensive. Hence, these carbon materials are not economical for large scale applications especially in wastewater treatment process [18].

We used an inexpensive, locally available and non-conductive charcoal to prepare conductive activated charcoal plate (ACP) as an easily made form of carbon material. The ability of ACP was investigated in decolorization of textile wastewater. The influence of effective variables including applied voltage, pH of the wastewater and contact time was studied in electrosorption process using response surface methodology (RSM). Moreover, the kinetics of the wastewater decolorization was studied. Finally, the regeneration of the ACP was investigated by applying reverse voltage.

EXPERIMENTAL PROCEDURE

1. Materials

Charcoal was obtained from a local market in Tabriz, Iran. Nitrogen and carbon dioxide gases were of analytical grade (Ehterami Co.). HCl and NaOH solutions used for pH adjustment were supplied by Merck.

2. Physico-chemical Analysis of the Wastewater

The textile wastewater was obtained from Farsh & Patu factory in Tabriz, Iran. It contains reactive orange 29 dye. The structure and characteristics of reactive orange 29 are given in Table 1. The physical and chemical specifications of the wastewater were analyzed for pH, turbidity, conductivity, chemical oxygen demand (COD), total suspended solids (TSS), total dissolved solids (TDS), sulfate

†To whom correspondence should be addressed.
E-mail: s_aber@tabrizu.ac.ir, soheil_aber@yahoo.com

Table 1. Structure and characteristics of reactive orange 29

Structure	Commercial name	Molecular weight (g mol^{-1})	Color index number
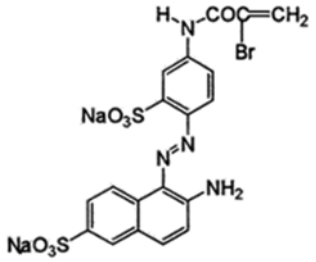	Lanasol orange G	599.34	13428

concentration, and ammonia concentration according to the methods summarized in the standard methods for the analysis of the wastewater [19].

3. Preparation and Characterization of ACP

The ACP was prepared from charcoal using physical activation method [20]. First, a piece of amorphous charcoal was cut in plate form with the dimensions of 1.1×3.4×5.7 cm^3 (15.91 g) and then placed in a tubular furnace. Temperature of the furnace was increased with raising rate of 5 min^{-1} up to 850 °C while the stream of N_2 gas flowed through the furnace. When the temperature of the furnace reached to 850 °C, N_2 stream was replaced by CO_2 gas to start the activation process. CO_2 stream flowed through the furnace at 850 °C for 1.5 h. Finally, CO_2 stream was replaced by N_2 gas and the produced ACP was cooled under N_2 atmosphere to room temperature. The prepared ACP was 1×3.1×5.2 cm^3 (10.45 g).

Surface morphology of the initial charcoal and the prepared ACP was observed with scanning electron microscope (SEM) model LEO 1430VP (Cambridge, UK). Meanwhile, the pore structure of the samples was analyzed with N_2 adsorption/desorption at 77 K by BELSORP-Mini (Japan) surface analyzer. Brunauer-Emmett-Teller (BET) equation was used to measure the total specific surface areas (S_{BET}) [21]. t-Plot theory was used to calculate total specific surface areas ($S_{t\text{-}Plot}$), micropore surface area (S_{mic}), external surface area (S_{ex}) and micropore volume (V_{mic}) [22]. Mesopore surface area (S_{mes}) and mesopore volume (V_{mes}) were derived from Barrett-Joyner-Halenda (BJH) method [23]. Also, micropore size (d_p) was calculated using micropore analysis (MP) method [24]. Fourier transform infrared (FT-IR) spectroscope (Bruker, TENSOR 27, Germany) with KBr pellet was used to study the surface functional groups of the charcoal and the ACP. Structural characterization of the ACP was determined by X-ray diffraction (XRD; Siemens D-500, Germany) using Cu Kα radiation (40 kV, 30 mA, and 0.15418 nm). Absorption spectrum of the textile wastewater was monitored by UV-Visible spectrophotometer (WPA light wave, S2000, England).

4. Experimental Set-up

Experimental set-up used for electrosorption experiments consisted of an electrosorption cell and a potentiostat (CV 320-xh, Hirad, Iran). The electrosorption cell consisted of a round Pyrex reactor containing wastewater and a conventional three-electrode system. The working, counter and reference electrodes were ACP, Pt plate (3×3 cm^2) and a saturated calomel electrode (SCE), respectively. Total wastewater volume was 90 mL in each experiment. The working and counter electrodes were separated by a 0.5-cm gap and immersed in 1-cm depth from the solution surface. pH of the wastewater was adjusted by HCl or NaOH solutions and measured using a pH meter (Eutech pH 510, Malaysia). A magnetic stirrer was used to keep constant mixing of the wastewater. Since real wastewater was used in this study, all of the electrosorption experiments were done without adding any electrolyte. The reactive orange 29 concentration in this solution was monitored with a UV-Visible spectrophotometer (Perkin-Elmer 550 SE, Germany) at 475 nm. Decolorization efficiency (%) was calculated from the following equation:

$$\text{Decolorization efficiency (\%)} = (C_0 - C_t)/C_0 \quad (1)$$

where C_0 and C_t (mg L^{-1}) are the initial and final concentration of reactive orange 29 in the wastewater at time t, respectively.

For kinetic experiments, 2 mL sample was withdrawn at predetermined time intervals and immediately after measuring the concentration of the residual reactive orange 29 in wastewater the sample was returned to the reactor. The amount of the dye adsorbed or electrosorbed per unit mass of the ACP, q_t (mg g^{-1}), at time t was determined by the following equation:

$$q_t = V(C_0 - C_t)/m \quad (2)$$

where V is the solution volume (L) and m is the ACP mass (g). Each experiment was carried out at least in duplicate.

5. Reusability of ACP

The reusability of the carbon materials will make the sorption process more economical. The reusability of the ACP was studied by using the electrodesorption in successive cycles of the wastewater decolorization. After each electrosorption experiment, the electrodesorption was conducted in 0.01 M NaOH solution with the volume of 90 mL and voltage of −450 mV. The electrodesorption process in each experiment lasted for 30 min. Then decolorization by electrosorption process was continued as a second cycle in a fresh wastewater. The same procedure was followed for subsequent cycles [25].

6. Experimental Design

To evaluate and predict the optimum operating conditions for desirable response, RSM is proposed as a kind of mathematical and statistical-based method. The RSM is an economic analytical approach due to the lessening of the number of tests compared to a full experimental design [26,27] . In this research, the optimal decolorization efficiency from the textile wastewater was obtained by the RSM in Design Expert 7.0 software. Voltage, pH, and contact

Table 2. Experimental ranges and levels of the independent test variables

Variables	Levels of independent variables				
	−2	−1	0	+1	+2
Voltage (X_1) (mV)	47.73	150	300	450	552.27
pH (X_2)	2.64	4	6	8	9.36
Time (X_3) (min)	39.55	60	90	120	140.45

time were taken as input (independent variables) and the decolorization efficiency was taken as response (dependent variable). Ranges and levels of the independent variables are presented in Table 2.

We used central composite design (CCD) which is the most frequently used form of the RSM to evaluate the singular and interacting influences of the three independent variables in 20 sets of experiments. These experiments were performed with two replicates in a randomized order to avoid systematic bias. The obtained data from decolorization efficiency (%) in each experiment were introduced into the Design Expert 7.0. Coded experimental values and corresponding responses are given in Table 3.

A second-order (quadratic) polynomial equation was used to fit the experimental results of the CCD according to the following equation:

$$Y = \beta_0 + \sum_{i=1}^{k} \beta_i X_i + \sum_{i=1}^{k} \beta_{ii} X_i^2 + \sum_{i=1}^{k-1} \sum_{j=2}^{k} \beta_{ij} X_i X_j + \varepsilon \quad (3)$$

where Y symbolizes the predicted response (decolorization efficiency), β_0 is constant term, β_i, β_{ii}, and β_{ij} are linear, quadratic and interaction coefficients, respectively. X_i, and X_j are input variables that influence the response (Y). i and j are index numbers for pattern and interaction terms (X_iX_j). They cannot have the same val-

Table 3. CCD experimental design table and the corresponding decolorization efficiencies (%) of the reactive orange 29

Run no.	Coded values of factors			Actual values of factors			Decolorization efficiency (%)
	Voltage (mV)	pH	Time (min)	Voltage (mV)	pH	Time (min)	
1	1	1	−1	450.00	8.00	60.00	30.41
2	1	1	1	450.00	8.00	120.00	36.09
3	0	0	0	300.00	6.00	90.00	29.17
4	0	1.682	0	47.73	6.00	90.00	19.53
5	−1	1	1	450.00	4.00	120.00	76.00
6	0	0	0	300.00	6.00	90.00	28.18
7	1	−1	−1	150.00	8.00	60.00	26.45
8	0	0	0	300.00	6.00	90.00	32.81
9	−1	−1	−1	150.00	4.00	60.00	29.42
10	−1	−1	1	150.00	4.00	120.00	42.52
11	0	0	−1.682	300.00	6.00	39.55	23.24
12	0	0	0	300.00	6.00	90.00	32.88
13	1.682	0	0	300.00	9.36	90.00	19.78
14	0	0	1.682	300.00	6.00	140.45	38.32
15	0	0	0	300.00	6.00	90.00	32.88
16	−1	1	−1	450.00	4.00	60.00	67.74
17	−1.682	0	0	300.00	2.64	90.00	56.12
18	0	1.682	0	552.27	6.00	90.00	55.38
19	0	0	0	300.00	6.00	90.00	35.35
20	1	−1	1	150.00	8.00	120.00	30.16

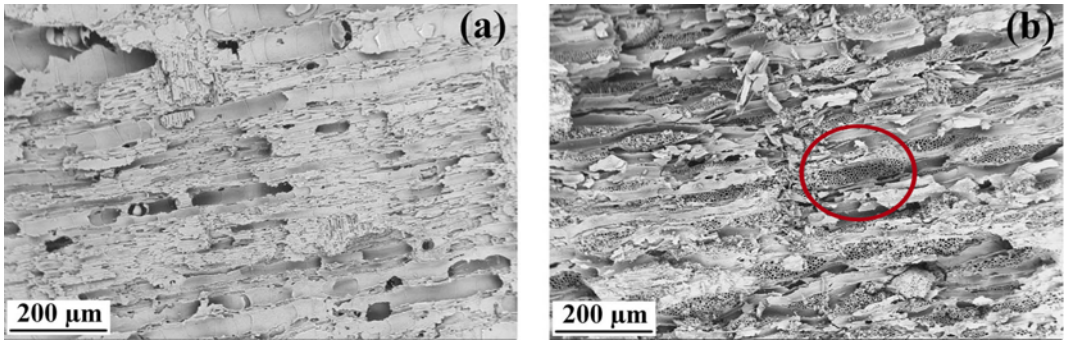

Fig. 1. SEM images of (a) the charcoal; (b) the ACP.

ues. ε represents statistical error and k is number of factors. The model was assessed by determination coefficient (*R*-squared) and *P*-value (probability) with 95% confidence level [28,29].

RESULTS AND DISCUSSION

1. Characterization of the Charcoal and ACP

Reaction of activation gas with precursor leads to production of pores and adsorption-effective functional groups on the surface of activated carbon [30]. Fig. 1(a) and (b) show SEM micrographs of the initial charcoal and the prepared ACP, respectively. As it can be seen, a large number of cavities and pores are found on the surface of the ACP. This is because in the presence of CO_2 as gaseous activation agent at high temperature, some carbon atoms of the charcoal are oxidized according to Eq. (4) and leave the charcoal surface, which leads to production of pores [31]. It is expected that higher adsorption capability is achieved due to the generated framework of the ACP in comparison with the charcoal.

$$C_{(s)}+CO_{2(g)}\rightarrow 2CO_{(g)} \quad (4)$$

FT-IR analysis was used to identify the functional groups of the charcoal and the ACP (Fig. 2). Fig. 2(a) shows FT-IR spectrum of the charcoal. According to Fig. 2(a), absorbance peak at about 3,443 cm^{-1} can be attributed to O-H stretching vibration. Two peaks at about 2,925 and 2,856 cm^{-1} are assigned to asymmetric C-H and symmetric C-H bonds, respectively. These two peaks along with two other weaker ones, 1,400 and 1,439 cm^{-1}, are correspondent to alkyl groups such as methyl and methylene groups [32]. Furthermore, the absorbance band around 1,600 cm^{-1} is ascribed to C=C stretching vibration [33]. Fig. 2(b) shows the FT-IR spectrum of the prepared ACP through activation of the charcoal at 850 °C. According to Fig. 2(b), C=O stretching vibration at about 1,647 cm^{-1} clearly appeared after activation of the charcoal [34]. O-H and N-H stretching between 3,300-3,500 cm^{-1} along with C=O stretching demonstrate the presence of carboxylic acid and amid on the surface of the charcoal after activation. Moreover, the appearance of absorption at about 1,068 cm^{-1} attributed to C-O stretching vibrations indicates formation of alcohol, phenol, acid, ether or ester groups on the ACP surface [35]. In fact, during the physical activation method in the presence of CO_2, some superficial carbon atoms of charcoal are oxidized incompletely and converted to chemical functional groups [36]. Based on these results, the existence and formation of oxygen-containing functional groups, such as hydroxyl and carbonyl groups in the porous surfaces of the ACP can affect the sorption behavior. Fig. 2(c) shows FT-IR spectrum of the prepared ACP after electrosorption of textile wastewater. Comparison of this spectrum with that of fresh ACP in Fig. 2(b) indicates the development of two new groups on the surface of ACP during electro-

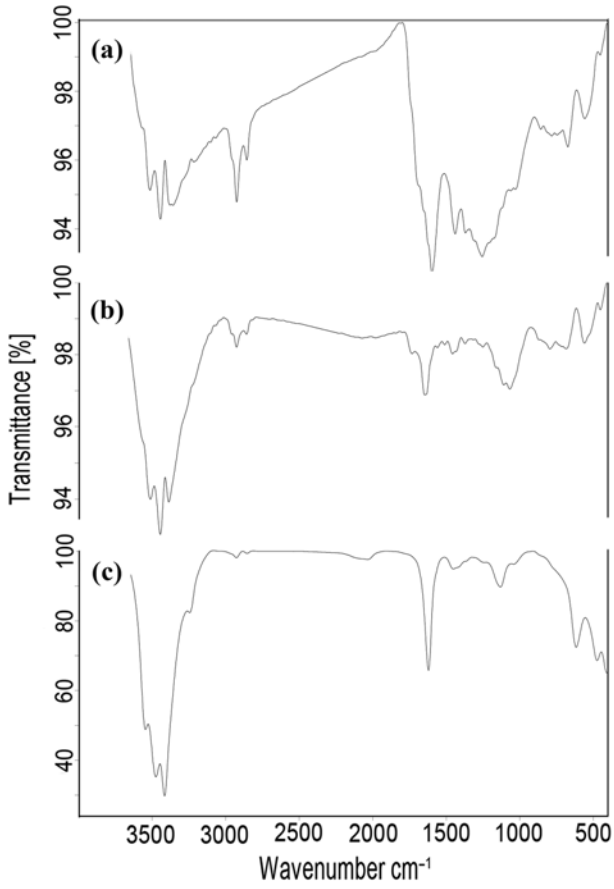

Fig. 2. FT-IR spectra of (a) the charcoal; (b) the ACP; (c) the ACP after electrosorption.

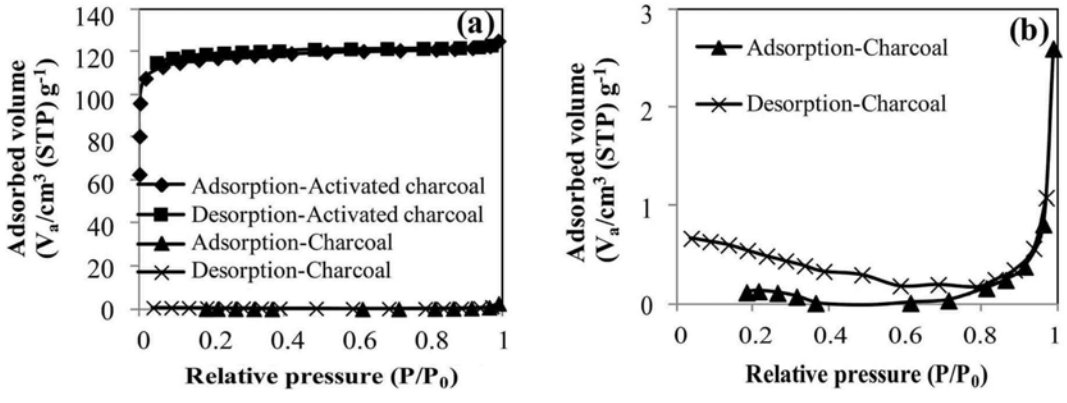

Fig. 3. (a) N_2 adsorption/desorption isotherms on the charcoal and the ACP; (b) N_2 adsorption/desorption isotherm on the charcoal with large magnification. V_a is the total gas volume adsorbed at the standard state (T=273.15 K and P=101.3 kPa).

sorption process. The new peaks around 1,132 cm^{-1} and 1,621 cm^{-1} are assigned, respectively, to the O=S=O asymmetric stretching vibration and C=C stretching vibration due to the presence of sulfate groups and aromatic rings in the reactive orange 29 molecules [37].

The N_2 adsorption/desorption isotherms for the charcoal and the ACP are shown in the relative pressure range of P/P_0=0-0.99 in Fig. 3. According to IUPAC classification [38], the charcoal followed type III isotherm, indicating that nonporous surface of the charcoal has very low adsorption ability, especially at lower relative pressures due to the weak interaction between adsorbate and sample surface (Fig. 3(b)). But, when the charcoal was activated at high temperature, the shape of the isotherm changed to type I. This type of isotherm implies that there is relatively strong interaction between adsorbate and sample surface that is primarily contributed by micropores (Fig. 3(a)).

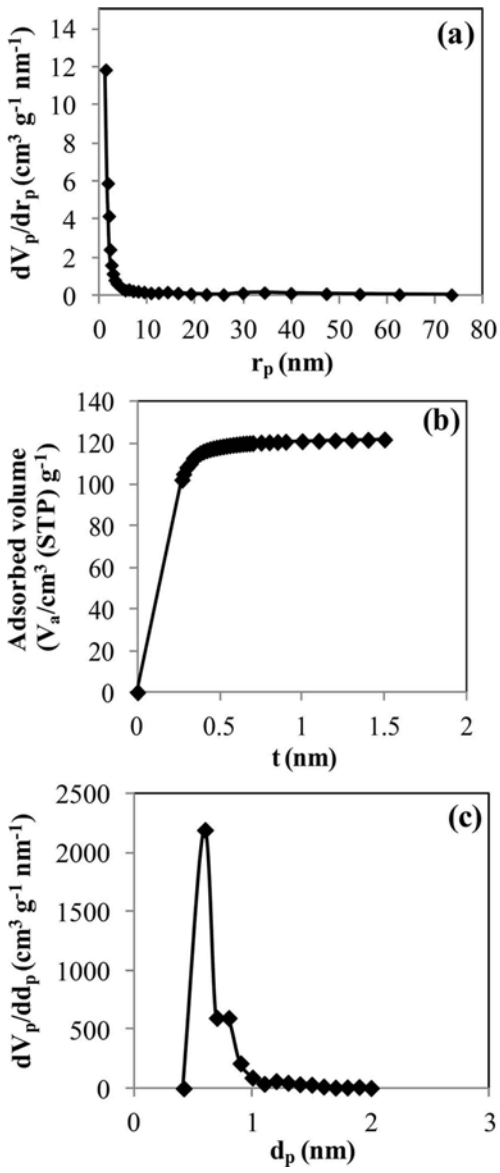

Fig. 4. (a) BJH pore volume distribution curve for the ACP. r_p is the pore radius; (b) t-Plot for the ACP. t is the average thickness of adsorbed layer; (c) MP-Plot for the ACP. d_p is micropore diameter.

BJH plot was illustrated for mesopore characterization (Fig. 4(a)). As can be seen, a sharp peak appears at 1.22 nm indicates the average pore size is 2.44 nm. In addition, analysis data for the mesopore surface area, S_{mes} (m^2 g^{-1}), and the mesopore volume, V_{mes}, (cm^3 g^{-1}) derived from BJH method are listed in Table 4.

The t-Plot was used to identify porosity distribution of the ACP using the average thickness of adsorbed layer (t). Fig. 4(b) shows that the obtained t-plot consists of two lines with different slopes, which means that the adsorbent has micropores [22]. In this case when micropores are completely occupied with N_2, the slope of t-Plot declines as curvature.

The curvature of t-plot was analyzed by MP method (Fig. 4(c)) to determine the micropore size (d_p) [24]. Based on the pore size distribution, most of the pores were smaller than 2 nm (0.6 nm). It indicates that the ACP dominantly is comprised of micropores, which is greatly beneficial for sorption.

Texture characteristics of the charcoal and the ACP along with analysis data obtained from the N_2 adsorption/desorption isotherms are summarized in Table 4. Comparison of BET surface area values of the charcoal and the ACP shows upon activation the amount of BET surface area of the charcoal increases and reaches as high as 461.67 m^2 g^{-1}, which is nearly 800 times greater than that of charcoal. This improvement in surface area is because the charcoal is activated in the atmosphere of CO_2. In the presence of this gas, some of the carbon atoms of the charcoal are oxidized. Complete car-

Table 4. Characteristics of the charcoal and the ACP (S_{BET} and $S_{t\text{-}Plot}$ are the total specific surface areas (m^2 g^{-1}) which were calculated by BET and t-Plot methods, respectively. S_{ex}: the external surface area (m^2 g^{-1}); S_{mic}: the micropore surface area (m^2 g^{-1}); V_{mic}: the micropore volume (cm^3 g^{-1}); S_{mes}: The mesopore surface area (m^2 g^{-1}); V_{mes}: the mesopore volume (cm^3 g^{-1}))

Characterization	Charcoal	ACP
S_{BET} (m^2 g^{-1})	0.58	461.67
$S_{t\text{-}Plot}$ (m^2 g^{-1})	[a]-	584.71
S_{ex} (m^2 g^{-1})	[a]-	3.49
[b]S_{mic} (m^2 g^{-1})	[a]-	581.22
V_{mic} (cm^3 g^{-1})	[a]-	0.18
S_{mes} (m^2 g^{-1})	[a]-	18.40
V_{mes} (cm^3 g^{-1})	[a]-	1.98×10^{-2}
C (%)	72.48	90.70
O (%)	27.52	9.30
H (%)	-	-
N (%)	-	-
Methylene blue adsorption value (mg g^{-1})	45.87	129.87
Ash content (wt%)	7.40	18.82

[a]According to IUPAC classification of adsorption isotherms, charcoal is considered to be a non-porous material and since t-Plot, MP-Plot, and BJH methods give information about microporous and mesoporous materials, the data obtained for the charcoal using these methods are not accurate

[b]$S_{mic}=S_{t\text{-}Plot}-S_{ex}$

bon oxidation leads to the development of micropore structure and consequently increase in pore volume and surface area [39]. Such a high surface area can promote the adsorption ability. Similarly, the activated carbon developed from surplus sewage sludge was prepared by Martin et al. [40]. The BET surface area of the dried sludge and sludge-based activated carbon was 3 and 253 $m^2 g^{-1}$, respectively.

As can be seen from Table 4, the specific surface areas obtained from BET and t-Plot methods are different for the ACP. It can be attributed to the hexagonal close-packed adsorption of adsorbate on the adsorbent surface according to t-plot assumption. Hexagonal close-packed adsorption considers more N_2 adsorption in unit area of adsorbent because of the packed placement of adsorbate molecules on the adsorbent surface. The microporous structure of the adsorbent is another assumption in the t-plot method and results in the estimation of higher specific surface area [22]. Micropores have adsorption capacities higher than macropores and mesopores. So, the specific surface area of the prepared ACP is in the range of 461.67 to 584.71 $m^2 g^{-1}$ obtained from BET and t-plot methods.

Elemental composition, methylene blue adsorption value and ash content of the charcoal and the ACP are listed in Table 4. Carbon and oxygen are the main elements of the samples and the elemental composition did not vary during the activation of the charcoal. Furthermore, comparison of methylene blue adsorption value of the charcoal and the ACP (Table 4) indicates that the adsorption ability of the ACP was higher than that of charcoal. This approves the development of adsorption effective porous structures during activation of the charcoal. Moreover, according to Table 4, the ash content of the ACP was higher than that of the charcoal, which can be attributed to oxidation and evaporation of organic materials during activation of the charcoal.

Electric conductivity of the charcoal before and after activation was also measured by four-point probe technique [41]. Comparison of the obtained electric conductivity for the charcoal and the ACP, which were respectively 3.93×10^{-6} (S m^{-1}) and 403.16 (S m^{-1}), proves that the activation process changes a non-conductive material to a conductive one. It is because the treatment of the charcoal at high temperatures changes the randomly oriented microcrystalline structure of the charcoal to a well-ordered structure. In this situation, crystallites have a large number of graphitic layers oriented parallel to each other. This can cause to increase the electric conductivity of the ACP [42].

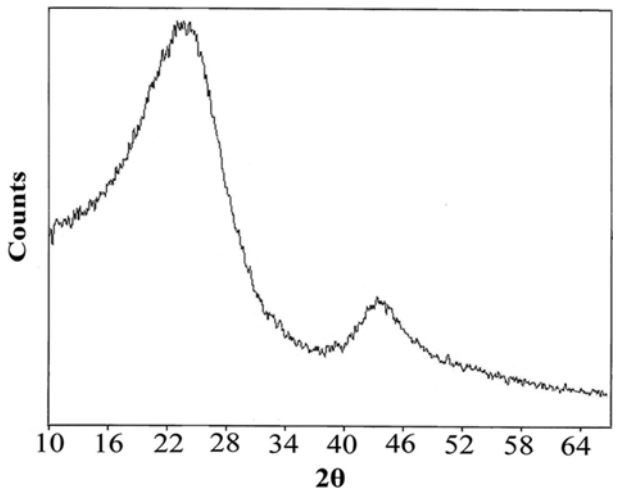

Fig. 5. XRD spectrum of the ACP.

Fig. 5 shows the XRD spectrum of the ACP. The 2θ values at 22° and 43.8° correspond to the reflection from graphite-like carbon, and its broadening suggests the possible presence of an amorphous phase within the ACP [43].

2. Model Fitting and Statistical Analysis

A second-order polynomial response equation in terms of dependent and independent coded variables was developed as follows according to the experimental results shown in Table 3:

$$\text{Decolorization efficiency} = 31.66 + 10.40X_1 - 11.25X_2 + 4.11X_3 - 7.74X_1X_2 - 0.36X_1X_3 - 1.50X_2X_3 + 3.39X_1^2 + 3.57X_2^2 + 1.03X_3^2 \quad (5)$$

Table 5 shows the analysis of variance (ANOVA) to determine the significant effect of the process variables on decolorization efficiency. The model *F*-value of 24.76 is higher than the critical *F*-value (3.02 at 95% significance level with degrees of freedom equal to 9 and 10). This confirms the significance of the model. The *P*-value of model is <0.0001, which is much lower than the critical value of 0.05. This also shows the model is significant.

Lack of fit *F*-value describes variation of the data around the fitted model [44]. In this work, lack of fit *F*-value of 4.31 for the quadratic model is lower than the critical *F*-value (5.05 at 95% significance level with degrees of freedom equal to 5 and 5). This confirms lack of fit is not significant relative to the pure error. The non-significant lack of fit implies the good predictability of the results obtained from the model. Moreover, a high value of determination coefficient (*R*-Squared) shows that the model can explain the response, successfully. In this work, the regression of the model has

Table 5. Estimated regression coefficients and ANOVA results from the data of CCD experiments

Source	Degree of freedom	F-value	P-value
Model	9	24.76	<0.0001
Linear			
X_1: Voltage (mV)	1	77.31	<0.0001
X_2: pH	1	90.58	<0.0001
X_3: Time (min)	1	12.08	0.0060
Square			
X_1X_1: Voltage (mV)×Voltage (mV)	1	8.69	0.0146
X_2X_2: pH×pH	1	9.61	0.0112
X_3X_3: Time (min)×Time (min)	1	0.81	0.3901
Interaction			
X_1X_2: Voltage (mV)×pH	1	25.09	0.0005
X_1X_3: Voltage (mV)×Time (min)	1	0.054	0.8215
X_2X_3: pH×Time (min)	1	0.94	0.3556
Residual Error	10		
Lack-of-fit	5	4.31	0.0674
Pure error	5		
Total	19		

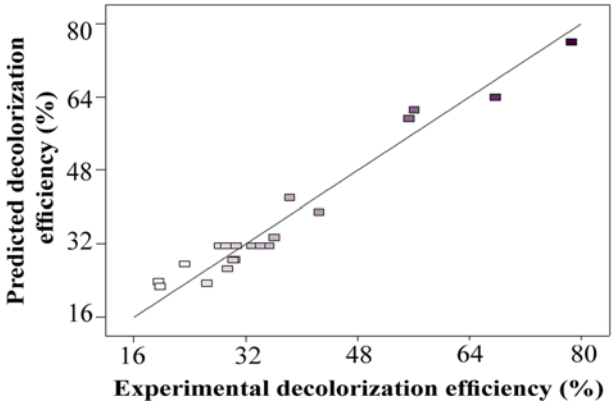

Fig. 6. Predicted vs. experimental decolorization efficiencies.

a fairly high value of *R*-Squared which is equal to 0.9571. The model adequacy was also verified with adjusted *R*-Squared values. The *R*-Squared of 0.9571 is in reasonable agreement with the adjusted *R*-Squared of 0.9184.

The accuracy of the model (Fig. 6) compares the predicted response values against the observed experimental ones for removal of reactive orange 29. The figure shows that the agreement between predicted and experimental results is acceptable. Consequently, the model can be used to predict the decolorization efficiecy in the design space.

Furthermore, according to P-values reported in Table 5 for each term of the introduced mathematical model, voltage (X_1), pH (X_2), time (X_3), the second-order effect of voltage (X_1^2), the second-order effect of pH (X_2^2) and the interaction between voltage and pH ($X_1 X_2$) were significant model terms.

3. Evaluation of Significant Model Terms

3-1. Effect of Voltage

Fig. 7 illustrates the effect of applied voltage on the decolorization efficiency of wastewater containing reactive orange 29. Electrosorption efficiency was increased with applying voltage. This observation is presumably due to the increase in adsorption rate as a result

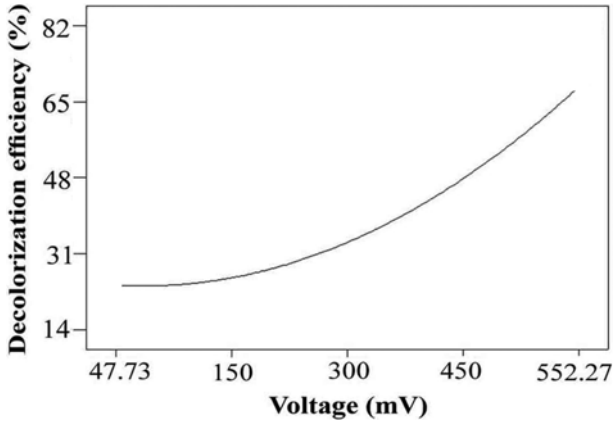

Fig. 7. The decolorization efficiency of reactive orange 29 vs. voltage. Constant conditions are pH=6 and contact time=90 min (all of the results related to the parameters were extracted from the model).

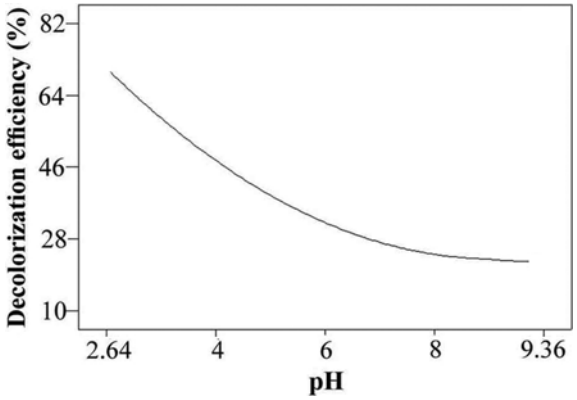

Fig. 8. The decolorization efficiency of reactive orange 29 vs. pH. Constant conditions are contact time=90 min and voltage =300 mV (All of the results related to the parameters were extracted from the model).

of increasing in the electrostatic interaction and affinity between surface of the ACP and ions. A behavior similar to this has also been observed in the electrosorption of alkali- and alkaline-earth cations using activated carbon electrode by Hou and Huang [9].

3-2. Effect of pH

Fig. 8 illustrates the effect of pH on the decolorization efficiency. The decolorization efficiency decreased with the increase of pH. It is due to strong electrosorption of negatively charged dye molecules on the positively charged ACP surface in acidic condition. At high pH values, the columbic repulsion between negatively charged dye molecules and ACP surface and also the competition between dye molecules and OH^- anions reduce the decolorization efficiency. A similar result was reported for electrosorption of thiocyanate anions on active carbon felt electrode in dilute solution by Rong and Xien [45].

3-3. Effect of Time and Kinetic Study

Fig. 9 shows the effect of contact time on decolorization efficiency of the wastewater. With increasing contact time, more dye molecules are electrosorbed on the surface of the ACP electrode, and consequently the decolorization efficiency increases.

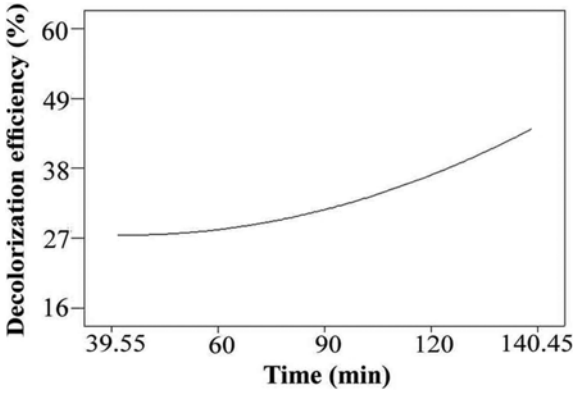

Fig. 9. The decolorization efficiency of reactive orange 29 vs. contact time. Constant conditions are pH=6 and voltage=300 mV (All of the results related to the parameters were extracted from the model).

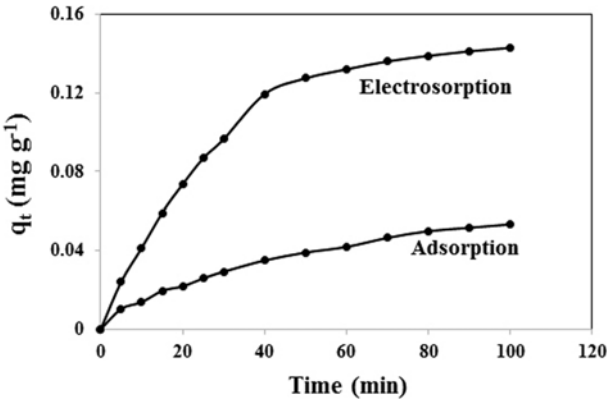

Fig. 10. Comparision of the adsorbed and the electrosorbed dye on the unit mass of the ACP at different contact times.

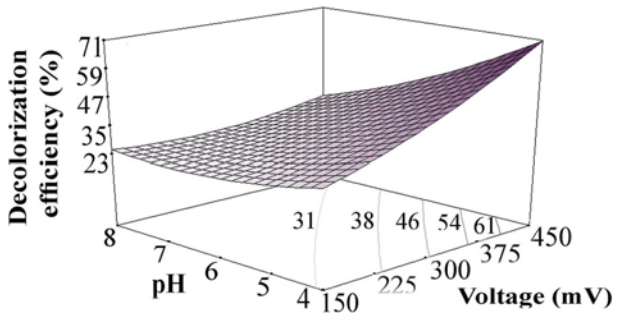

Fig. 11. Contour and surface plots showing the interaction of pH and voltage (contact time=90 min).

To investigate the ACP electrosorption behavior quantitatively, kinetic studies of the wastewater decolorization were done at two different situations: without applying the potential (adsorption) and with applying the potential of 450 mV while the other variables were the same. Values of the adsorbed and electrosorbed dye on the unit mass of the ACP at different contact times were ploted versus time (Fig. 10). Comparison of the obtained results shows that at all investigated contact times, the amount of the electrosorbed dye was higher than that of adsorbed dye. This indicates possitive effect of the applied voltage on sorption ability of the ACP.

The sorption rate constants were determined from the linear form of the pseudo-first order (Eq. (6)) and pseudo-second order (Eq. (7)) kinetic models [46,47].

$$\ln(q_e - q_t) = \ln q_e - k_1 t \tag{6}$$

$$\frac{t}{q_t} = \frac{1}{k_2 q_e^2} + \frac{t}{q_e} \tag{7}$$

where q_e (mg g^{-1}) is the amount of adsorbed or electrosorbed dye on unit mass of the ACP at equilibrium time. Also, k_1 (min^{-1}) and k_2 (g mg^{-1} min^{-1}) are adsorption or electrosorption rate constants of the pseudo-first order and the pseudo-second order kinetic models, respectively. Table 6 lists the electrosorption and adsorption rate constants and the related correlation coefficients (R^2). For both the electrosorption and adsorption processes, the pseudo-first order kinetic model can fit the experimental data better than the pseudo-second order model due to the higher values of the R^2. Furthermore, comparison of the rate constants (k_1) calculated for electrosorption and adsorption from the pseudo-first order model shows that the sorption capacity and the rate constant increased by applying the voltage of 450 mV due to the increase in the electrostatic forces between ionic forms of adsorbates and the ACP surface. These results are in agreement with the adsorption/electrosorption of NaCl from aqueous solutions on activated carbon electrode surface by Chen et al. [48].

Table 6. Comparison of the adsorption and the electrosorption kinetic data in the wastewater decolorization using the ACP electrode

	Pseudo-first order			Pseudo-second order		
	q_e	k_1	R^2	q_e	k_2	R^2
Adsorption	0.35	0.0242	0.9916	0.07	0.47	0.9072
Electrosorption	6.40	0.042	0.9964	0.18	0.23	0.9433

4. Response Surface and Contour Plots

The response surface and contour plots were used to show the effect of interaction between investigated variables on electrosorption process. Fig. 11 displays the combined effect of pH and voltage as significant model terms while amounts of other variables were considered in central points. The highest decolorization efficiency was obtained with minimum level of pH, but with maximum level of voltage.

5. Optimization and Model Validation

Based on the combination of all response surfaces, optimum conditions were a voltage of 450 mV, pH of 4, and contact time of 120 min. The predicted decolorization efficiency at optimum conditions was equal to 74.29%, a good result for the complicated matrix of real wastewater. An average decolorization efficiency of 76% was obtained from three replicates of decolorization experiments at optimum conditions. The good agreement between the predicted and the experimental values confirms the validity of the CCD model in this work.

Table 7. Characteristics of the raw textile wastewater and the decolorized textile wastewater

Parameters	Raw wastewater	Decolorized wastewater
Initial dye concentration	28	-
pH	6.8	4
Turbidity (FTU)	8	3
Conductivity (mS cm^{-1})	4.09	2.92
COD	420	310
TDS	2404	2020
TSS	512	226
Chloride	609	322
Sulfate	170	115
Ammonia	4.1	Nil

All the values except pH, turbidity and conductivity are expressed in mg L^{-1}

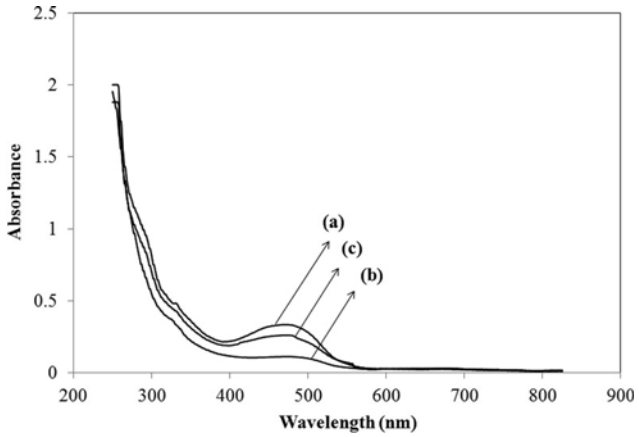

Fig. 12. UV-visible absorption spectra of (a) raw textile wastewater; (b) textile wastewater after electrosorption; (c) the solution contains pollutants electrodesorbed from the surface of the used ACP.

6. Wastewater Characteristics

The characteristics of textile wastewater before and after decolorization by electrosorption are shown in Table 7. As it can be seen from this table, the values of all measured parameters decreased after electrosorption at optimum conditions. This means that the prepared ACP was efficient not only in decolorization but also in reduction of the main parameters of the wastewater during the electrosorption process.

7. UV-visible Spectrum of Textile Wastewater

Fig. 12(a), (b) and (c) show the absorption spectra of the raw wastewater, the electrosorbed wastewaters, and the solution contains pollutants electrodesorbed from the surface of the used ACP, respectively. The UV-Visible spectrum of the textile wastewater after electrosorption at optimum conditions shows that the absorption peak around 475 nm corresponding to reactive orange 29 decreased through treatment process (Fig. 12(b)). The loss of absorbance is due to the removal of dye from the wastewater. No new absorption peak appeared in the spectrum of the electrosorbed textile wastewater. This indicates that no chemical destruction occurred during the electrosorption of the reactive orange 29 on the surface of the ACP. Furthermore, the spectrum of the solution contains electrodesorbed pollutants shows the absorbance peak at 475 nm with considerable intensity (Fig. 12(c)). This implies that there was no chemical degradation in the textile wastewater during the electrosorption process.

8. Regeneration of the ACP Electrode by Electrodesorption

The results obtained from investigation of the prepared ACP electrode ability in five successive electrosorption cycles were illustrated in Fig. 13. As can be seen, the electrosorption efficiency of the ACP decreased slightly from the first to the second cycle. It is probably due to irreversible sorption of dye on ACP interior pores. However, at second to the fifth cycles, the amount of decolorization was almost identical and the electrode displayed a stable behavior. This is probably due to the fact that with applying the reverse voltage, almost all of the electrosorbed ions release from the surface of the electrode into the solution. This demonstrates that the ACP has high reusability without obvious changes in the electrosorption ability and is a promising sorbent for decolorization of the real wastewater. A similar result was reported for NaCl electrosorption/electrodesorption on mesoporous activated carbon electrode by Wang et al. [18].

CONCLUSION

The ACP exhibits promising results in wastewater decolorization due to its developed porosity, high conductivity and easy operation. It can undergo five successive electrosorption/electrodesorption cycles without significant loss in decolorization efficiency. RSM approach is an appropriate method to analyze the electrosorption process with respect to various effective variables including applied voltage, pH, and contact time. The adsorption and electrosorption of reactive orange 29 on the ACP electrode follow a pseudo-first order kinetic model. The amount of the electrosorbed dye and rate constant of the electrosorption process are, respectively, about 18 and 1.7 times greater than the related parameters in the adsorption process. The UV-Visible spectra confirm the sorption of the dye from the textile wastewater.

ACKNOWLEDGEMENT

This paper is published as part of a research project supported

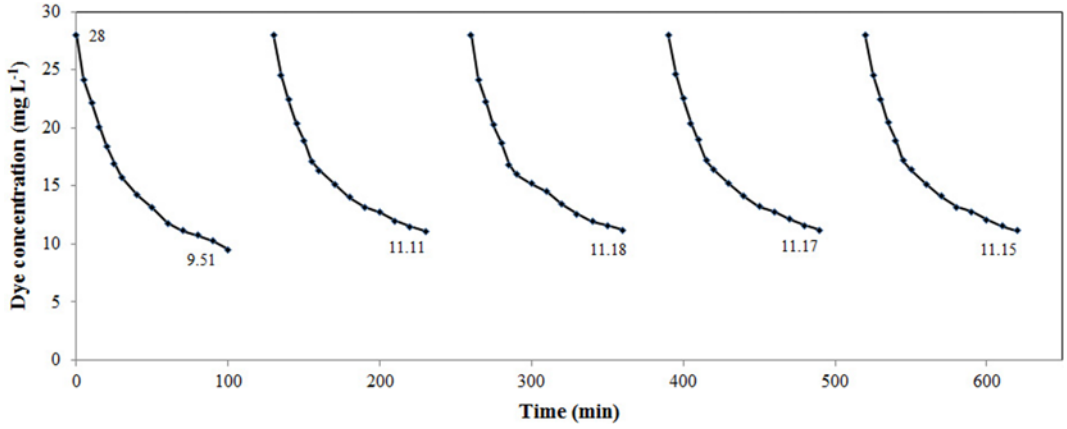

Fig. 13. Successive electrosorption/electrodesorption cycles of the textile wastewater by the same ACP electrode.

by the University of Tabriz Research Affairs Office. The authors would like to express their gratitude to the University of Tabriz for financial and other supports provided in the implementation of this research project.

REFERENCES

1. M. M. Hossain, M. I. Mahmud, M. S. Parvez and H. M. Cho, *Environ. Eng. Res.*, **18**, 157 (2013).
2. S. Karthikeyan, A. Titus, A. Gnanamani, A. B. Mandal and G. Sekaran, *Desalination*, **281**, 438 (2011).
3. S. Aber, D. Salari and B. Ayoubi Feiz, *Water Sci. Technol.*, **63**, 1389 (2011).
4. M. K. Mondal, *Korean J. Chem. Eng.*, **27**, 144 (2010).
5. M. Shirzad-Siboni, S.-J. Jafari, M. Farrokhi and J. K. Yang, *Environ. Eng. Res.*, **18**, 247 (2013).
6. A. Ban, A. Schafer and H. Wendt, *J. Appl. Electrochem.*, **28** 227 (1998).
7. K. Y. Foo and B. H. Hameed, *J. Hazard. Mater.*, **170**, 552 (2009).
8. Y. Zhan, C. Nie, H. Li, L. Pan and Z. Sun, *Electrochim. Acta*, **56**, 3164 (2011).
9. C.-H. Hou and C.-Y. Huang, *Desalination*, **314**, 124 (2013).
10. C.-C. Huang and J.-C. He, *Chem. Eng. J.*, **221**, 469 (2013).
11. H. M. A. Asghar, S. N. Hussain, H. Sattar, E. P. L. Roberts and N. W. Brown, *Korean J. Chem. Eng.*, **31**, 834 (2014).
12. E. Ayranci and B. E. Conway, *J. Electroanal. Chem.*, **513**, 100 (2001).
13. Y. Kong, W. Li, Z. Wang, C. Yao and Y. Tao, *Electrochem. Commun.*, **26**, 59 (2013).
14. Y. Han, X. Quan, S. Chen, H. Zhao, C. Cui and Y. Zhao, *Sep. Purif. Technol.*, **50**, 365 (2006).
15. Y. Zhan, C. Nie, H. Li, L. Pan and Z. Sun, *Phys. Status Solidi*, **9**, 55 (2012).
16. H. Li, T. Lu, L. Pan, Y. Zhang and Z. Sun, *J. Mater. Chem.*, **19**, 6773 (2009).
17. J. C. Farmer, S. M. Bahowick, J. E. Harrar, D. V. Fix, R. E. Martinelli, A. K. Vu and K. L. Carroll, *Energy Fuels*, **11**, 337 (1997).
18. G. Wang, B. Qian, Q. Dong, J. Yang, Z. Zhao and J. Qiu, *Sep. Purif. Technol.*, **103**, 216 (2013).
19. A. P. H. Association, *Standard Methods for the Examination of Water and Wastewater*, Washington D.C., USA (1989).
20. S. Aber and M. Sheydaei, *Clean - Soil Air Water*, **40**, 87 (2012).
21. S. Brunauer, P. H. Emmett and E. Teller, *J. Am. Chem. Soc.*, **60**, 309 (1938).
22. B. C. Lippens and J. H. de Boer, *J. Catal.*, **4**, 319 (1965).
23. E. P. Barrett, L. G. Joyner and P. P. Halenda, *J. Am. Chem. Soc.*, **73**, 373 (1951).
24. R. S. Mikhail, S. Brunauer and E. E. Bodor, *J. Colloid Interface Sci.*, **26**, 45 (1968).
25. S. Karthikeyan, C. J. Magthalin, A. B. Mandal and G. Sekaran, *RSC Advances*, **4**, 19183 (2014).
26. M. Sheydaei and S. Aber, *CLEAN - Soil, Air, Water*, **41**, 890 (2013).
27. S. Dey and S. Mukherjee, *J. Environ. Sci.*, **25**, 698 (2013).
28. S. Murugesan, S. Rajiv and M. Thanapalan, *Korean J. Chem. Eng.*, **26**, 364 (2009).
29. S. Y. Chun, S. W. An, S. J. Lee, J. T. Kim and S. W. Chang, *Korean J. Chem. Eng.*, **31**, 994 (2014).
30. A. Afkhami, T. Madrakian and Z. Karimi, *J. Hazard. Mater.*, **144**, 427 (2007).
31. A. Aworn, P. Thiravetyan and W. Nakbanpote, *J. Anal. Appl. Pyrolysis*, **82**, 279 (2008).
32. S. Aber, A. Khataee and M. Sheydaei, *Bioresour. Technol.*, **100**, 6586 (2009).
33. Q. Shi, J. Zhang, C. Zhang, C. Li, B. Zhang, W. Hu, J. Xu and R. Zhao, *J. Environ. Sci.*, **22**, 91 (2010).
34. S. Karthikeyan, C. Anandan, J. Subramanian and G. Sekaran, *RSC Advances*, **3**, 15044 (2013).
35. S. Karthikeyan, R. Boopathy, V. K. Gupta and G. Sekaran, *J. Mol. Liq.*, **177**, 402 (2013).
36. Z.-M. Wang, H. Kanoh, K. Kaneko, G. Q. Lu and D. Do, *Carbon*, **40**, 1231 (2002).
37. G. Vijayakumar, C. K. Yoo, K. G. P. Elango and M. Dharmendirakumar, *Clean*, **38**, 202 (2010).
38. K. S. W. Sing, *Pure Appl. Chem.*, **54**, 2201 (1982).
39. S. Karthikeyan, M. Anil Kumar, P. Maharaja, T. Partheeban, J. Sridevi and G. Sekaran, *J. Taiwan Inst. Chem. E.*, **45**, 1739 (2014).
40. M. J. Martin, A. Artola, M. D. Balaguer and M. Rigola, *Chem. Eng. J.*, **94**, 231 (2003).
41. W. R. Runyan, *Semiconductor Measurements and Instrumentation*, McGraw-Hill, New York (1975).
42. R. C. Bansal and M. Goyal, *Activated Carbon Adsorption*, CRC Press, Boca Raton, FL (2005).
43. S. Karthikeyan and G. Sekaran, *Phys. Chem. Chem. Phys.*, **16**, 3924 (2014).
44. F. Shahrezaei, Y. Mansouri, A. A. L. Zinatizadeh and A. Akhbari, *Powder Technol.*, **221**, 203 (2012).
45. C. Rong and H. Xien, *J. Colloid Interface Sci.*, **290**, 190 (2005).
46. Y. S. Ho and G. McKay, *Process Biochem.*, **34**, 451 (1999).
47. S. J. Allen, Q. Gan, RonanMatthews and P. A. Johnson, *J. Colloid Interface Sci.*, **286** 101 (2005).
48. Z. Chen, C. Song, X. Sun, H. Guo and G. Zhu, *Desalination*, **267**, 239 (2011).